ELSEVIER

International Journal of Heat and Fluid Flow 23 (2002) 533–543

International Journal of HEAT AND FLUID FLOW

www.elsevier.com/locate/ijhff

Characterisation of a coupled phenomenon in a confined shear-layer

J. Vetel, F. Plourde *, S. Doan-Kim

Laboratoire d'Etudes Thermiques, University of Poitiers, UMR CNRS 6608, BP 40109, 86961 Futuroscope Cedex, France

Received 18 September 2001; accepted 17 November 2001

Abstract

Experimental measurements in a confined chamber with injection through porous walls were carried out over a range of low characteristic velocity levels in order to analyse the vortex shedding phenomenon in the wake of an emerging obstacle and its coupling with the confined chamber acoustics. Two trends were identified at subsonic velocities. At lower velocities, a weak coupling was observed and the hydrodynamics could force a shifting of the resonant acoustic frequency. Turbulence behaviour greatly influenced the dissipation of coherent structures. Nevertheless, the coupling phenomenon strengthened at higher velocities. It caused the natural self-sustained shear-layer to align with the first longitudinal acoustic mode and generated a complete resonant state in the whole chamber. © 2002 Elsevier Science Inc. All rights reserved.

1. Introduction

Unstable developments in confined flows have been studied and results clearly show that coupling phenomena between hydrodynamics and acoustics were at the origin of the unstable behaviour. Brown et al. (1981) demonstrated that significant amplification of coupling phenomena can be reached and pointed out that two conditions are necessary to produce noise: the existence of an unsteady flow such as a jet or shear-layer, and the impingement of such a flow on an obstacle. This complex mechanism was also observed both in confined and in open spaces, as were the impact of a circular jet upon an edge, the impingement of vorticity concentrations upon a corner and the oscillations induced by flows over cavities. Ho and Nosseir (1981) used a high speed subsonic jet impinging on a flat plate in order to highlight the feed-back loop phenomenon. In fact, this feed-back loop consists of downstream convected coherent structures and upstream propagating pressure waves generated by the impingement of coherent structures on the plate. The upstream propagating waves excite the thin shear-layer near the nozzle lip and produce periodic coherent structures. Ziada and Rockwell (1982) conducted experiments in which mechanisms of coherent structure impingement on the edge induced forced on the wedge. The nature of the vortex–wedge interaction and of the associated force on the wedge were directly related to the induced velocity at the upstream separation edge, providing the essential feedback for self-sustained oscillations. Tang and Rockwell (1982) underlined the strong dependence of the vortex–corner interaction. The frequency of oscillation is typically expressed by the Strouhal number St. Rockwell and Naudascher (1979) presented frequency jumps and the occurrence of several stages in the Strouhal number evolution. Furthermore, it was shown that the resonance phenomenon between shear-layer oscillations and upstream pressure waves may be enhanced by an acousticor by a free-surface standing wave. Hourigan et al. (1990), Isaacson and Marshall (1982) and Dunlap and Brown (1981) studied shear-layer oscillations in a confined area containing sets of baffles and commented on the effect of non-linear resonant energy transfer. The oscillation frequency depends strongly on the Strouhal number. In addition to the critical Strouhal number, the position of the baffles relative to the acoustic mode structure is an important parameter depending on the obstacle location with regard to the acoustic velocity node or velocity antinode.

The aim of our study is to understand the complex behaviour of the flow in a confined chamber with porous wall injection and to highlight conditions for

* Corresponding author.
E-mail address: plourde@let.ensma.fr (F. Plourde).

0142-727X/02/$ - see front matter © 2002 Elsevier Science Inc. All rights reserved.
PII: S0142-727X(01)00151-5

Nomenclature

a	$=\sqrt{\gamma rT}$, sonic velocity (m/s)
f_{nL}	$=na/2L$, nth longitudinal acoustic mode (Hz)
h_t	height of the nozzle throat (m)
h_c	channel height (m)
L	channel length (m)
P	mean pressure at the front-head (Pa)
P'	fluctuating pressure (Pa)
q_m	mass flow rate (kg/s)
s	$=wh_c$, characteristic surface area (m^2)
T	temperature of the flow (K)
u_c	coherent structure velocity (m/s)
u_v	$=q_m/\rho s$, characteristic velocity based on the mass flow rate (m/s)
u'	characteristic fluctuation velocity (m/s)
v_w	wall injection velocity (m/s)
w	channel width (m)
X, Y, Z	non-dimensional axis normalised respectively by L, h_c and w
τ	time delay (s)
μ	dynamic viscosity (kg/ms)
ρ	density (kg/m^3)

Dimensionless parameters

M	Mach number
Re_c	$=\rho u_v h_c/\mu$, Reynolds number
Re_w	$=\rho v_w h_c/\mu$, wall injection Reynolds number
$R_{u'p'}(\tau)$	temporal correlation coefficient of the pressure and the velocity fluctuations
St	Strouhal number
γ	specific heat ratio

the presence of a hydrodynamic–acoustic coupling phenomenon. For this purpose, pressure fluctuations at the head-end of the chamber were recorded and analysed in order to underline possible unstable behaviour and were correlated with velocity fluctuations. Couton et al. (1999) already stated on the presence of a non-linear amplification with the increase of mass flow rate as well as of the Mach number and Couton et al. (1997) also numerically demonstrated a strong coupling. But, this present study focuses essentially on the shear-layer self-sustained oscillations, specifically following coherent-structure shedding in the wake of an emerging obstacle and impingement area, with regard to the internal velocity levels in the chamber. A wide range of velocity levels has been studied to analyse the influence of the flow field on the coupling phenomenon and acoustic interference. An analytical model was proposed in order to analyse and to understand the presence of the coupling phenomenon.

2. Experimental set-up and measuring techniques

2.1. Test channel

The principle of the test channel has been fully described in previous works by Couton et al. (1996), but the main features are briefly summarised. In order to simulate potential mechanisms in solid-propellant rocket motors, some essential features of both hydrodynamic and geometric design of the internal chamber were reproduced. In terms of internal design, the test channel (Fig. 1) was a non-symmetric 2D channel 0.623 m long (L), 0.05 m wide (w) and 0.028 m high (h_c). The channel was composed of three injection blocks whose lengths were 0.064 m for the first, 0.253 m for the second and 0.264 m for the third one. The simulation of the combustion was performed by injecting air at ambient temperature through the porous walls of the blocks. A feeding system provided an accurate mass flow injection

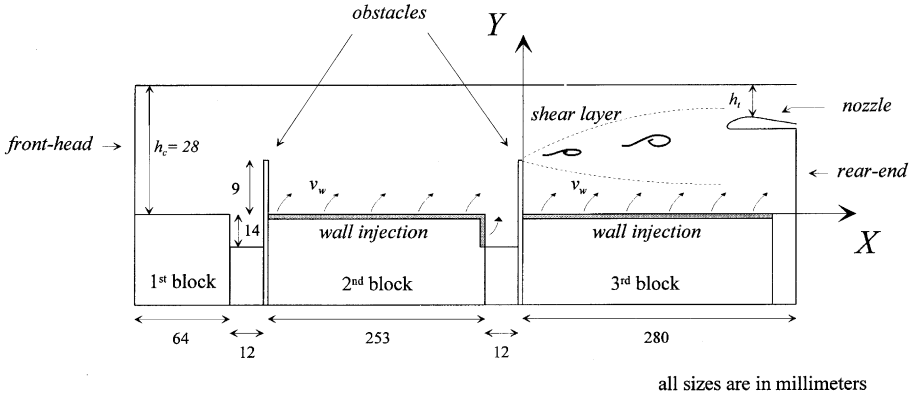

Fig. 1. Experimental configuration.

rate through porous walls and ensured a constant injection velocity v_w all along the blocks. In all the results presented in this paper, the first block was not fed with air. This block represented the ignition propellant block that burns rapidly. As shown in Fig. 1, between each block, i.e. between the first and the second block and between the second and the third block, an obstacle emerged above the porous walls. As there was no air injection through the first block, we focused our velocity study on the second obstacle and within its wake. The head-end was closed while a submerged nozzle was located at the rear-end. The height h_t of the throat could be varied in order to modulate the characteristic Mach number inside the chamber. The porous walls were mainly characterised by a sintered-bronze sphere Poral plate with a 2 μm characteristic diameter to isolate the flow in the chamber while the sonic conditions at the nozzle throat ensured the acoustic isolation of the channel from the exterior environment. In terms of hydrodynamics, the 1/40 scale model was based on a solid rocket motor with the conservation of Mach and Strouhal numbers. Since the objective of this study was to understand the influence of the mean velocity level u_v inside the chamber, the total mass flow rate q_m was fixed at 0.065 kg/s while the height of the nozzle varied from 2 to 4 mm. The nozzle throat was progressively closed step by step at intervals of 0.05 mm, which imposed a mean pressure change from 3.4×10^5 to 1.43×10^5 Pa. Thus, the variation range of mean velocity level u_v was from 12 to 30 m/s. The complete details of the experimental conditions are given in Table 1.

2.2. Measurement techniques

The measurements of the mean pressure and of its fluctuating component were made at the head-end with a piezo-electric quartz transducer, whose sensitivity was about 10 Pa and its cut-off frequency was 13 kHz. For every pressure measurement, more than 200,000 samples were recorded at a 10 kHz frequency and spectral analysis decomposition was made with blocks of 4096 data. This allowed an estimate of the spectral energy response with an error $<5\%$.

Table 1
Experimental conditions

Front-head pressure P	1.43×10^5–3.40×10^5 Pa
Mass flow rate q_m	0.065 kg/s
Characteristic mean velocity u_v	12–30 m/s
Mach range	0.035–0.086
Global Strouhal number St	2.23–5.60
Characteristic Reynolds number Re_c	71,300
Wall injection Reynolds number Re_w	3,800
Air temperature	298 K
Mode f_{1L}	278 Hz
f_{2L}	556 Hz

The injected air temperature was controlled by a K-thermocouple in order to precisely evaluate the sonic velocity a in the chamber. The accuracy of the thermocouple was 0.5 °C which induced an accuracy of 0.08% for the evaluation of a.

Velocity measurements were conducted with a 5 μm single miniature wire. The frequency response of the hot-wire system was found to be ≈100 kHz and the analog signal from the anemometer was digitised through a 16-bit resolution analog to digital converter. Data were directly analysed in conjunction with a relevant calibration. The calibration of the probe was carried out with 40 different velocity levels from 4 to 60 m/s at normal pressure level. From the hot-wire calibration equation and data acquisition, the uncertainty of the mean velocity was $<2\%$ and of the fluctuating velocity 5%. Furthermore, The Reynolds number Re_c, based on the mean velocity level u_v and the channel height h_c was maintained constant even when u_v strongly increased. In fact, the characteristic Reynolds number Re_c may be written as $q_m/w\mu$.

As shown in Fig. 1, a cartesian co-ordinate system (X, Y, Z) was chosen with its origin located at the bottom of the obstacle and with the X-axis oriented along the main flow direction. For the purpose of the present study, all velocity measurements reported were recorded at the centre of the chamber, i.e. for $Z = 0$. Furthermore, X and Y were normalised with the length between the location of the obstacle and the rear-end of the chamber for X, i.e., 280 mm, and with the height of the channel for Y, i.e., 28 mm.

3. Mean velocity influence on the internal flow characteristics

3.1. Fluctuating pressure field

The variation of the root-mean-square of the pressure fluctuations $\sqrt{\overline{P'^2}}$, measured from the front-head transducer, with u_v is presented in Fig. 2. Two different amplification stages are noted. The first, Stage I, extends from u_v levels of 12–26 m/s and a gradual linear increase of $\sqrt{\overline{P'^2}}$ is observed concurrently with the increase of the mean velocity. This increase was obtained with an increasing throat height h_t because, with a fixed mass flow rate q_m, the sonic nozzle condition controlled the velocity as well as the pressure in the chamber according to the nozzle height h_t. In Stage I, the ratio of the pressure fluctuations $\sqrt{\overline{P'^2}}$ and the mean pressure P at the front-head varied from 0.001 to 0.01%. The second stage, Stage II, is mainly characterised by a higher increase of $\sqrt{\overline{P'^2}}$ with increasing u_v. For $26 \leqslant u_v \leqslant 28$ m/s, an abrupt change in the root-mean-square pressure fluctuations occurs and beyond theses values, the change is also

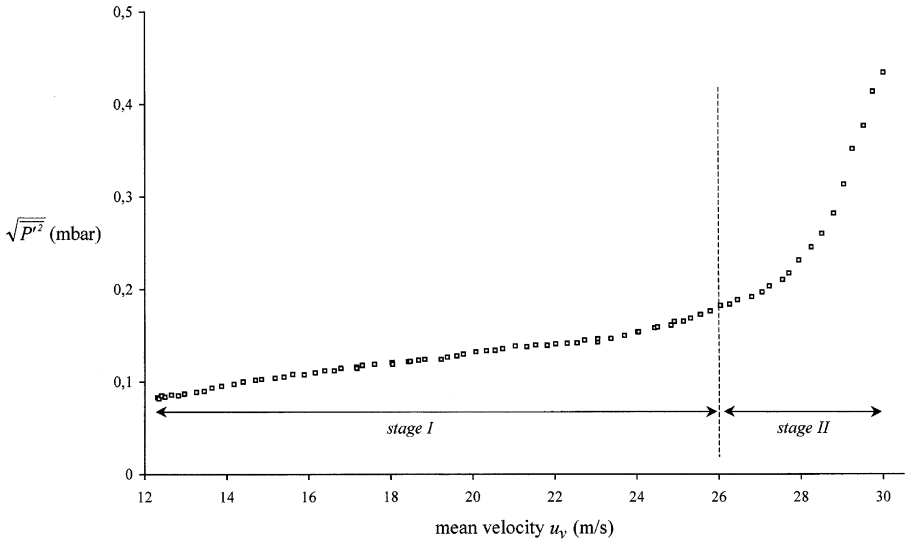

Fig. 2. Root-mean-square of pressure fluctuations at head-end versus mean velocity level u_v.

linear but displays a characteristic slope 30 times as high as that of the first stage. Nevertheless, pressure fluctuations collected at the front-head remain very low compared to the values of the average pressure. For instance, the $\sqrt{\overline{P'^2}}/P$ ratio reached 0.07% at the maximum mean velocity u_v of 30 m/s. In order to analyse these differences in amplification, the spectral analysis of the pressure fluctuations was performed.

Representative frequency spectra of the front-head pressure fluctuations are shown in Fig. 3, where u_v is presented for each spectrum. Each amplification stage is illustrated by frequency spectra. For instance, at $u_v = 16.5$ m/s, the spectrum is mainly characterised by the presence of one single peak. The complete fluctuation energy is concentrated at a fundamental frequency of 270 Hz. This frequency is close to the theoretical fundamental longitudinal acoustic mode f_{1L}. In fact, noise created by the flow in the confined chamber matches up with the internal acoustics. In the transition between Stages I and II, the shapes of spectra do not change radically. Amplification of the root-mean-square of the pressure fluctuations organises itself mostly at the fundamental frequency (f_{1L}), even if a weak energy concentration can be seen at the second harmonic frequency (≈540 Hz), for $u_v = 26.5$ m/s and most evidently in Stage II. For $u_v \geqslant 29$ m/s, the first four harmonic frequencies are present in the pressure fluctuations but spectra obtained are always mostly characterised by increasing fluctuating energy around the first longitudinal acoustic mode. The magnitudes and frequencies of the first and second dominant spectral peaks are plotted in Fig. 4 for a complete range of mean velocity values ($9 < u_v < 30$ m/s).

First of all, as already underlined above, the magnitudes of the highest peak close to the first longitudinal acoustic mode exceed all others, specifically the second

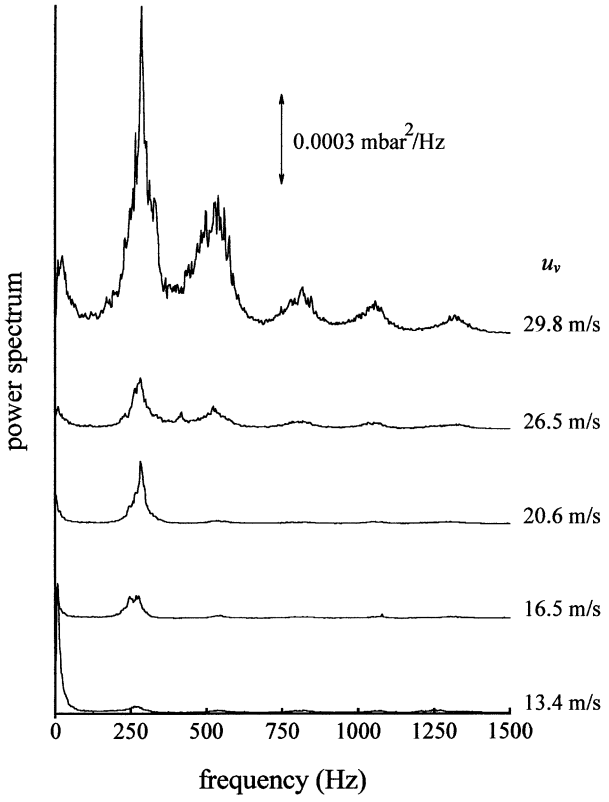

Fig. 3. Change of the pressure spectral response versus mean velocity level u_v.

acoustic longitudinal mode, whatever the velocity level u_v. But the change in the fluctuation energy of the fundamental frequency f_{1L} does not increase linearly. A maximum of energy at the first longitudinal acoustic mode f_{1L} is obtained for approximately $u_v = 17$ m/s, i.e. at Stage I, and then a steep rise is observed beyond the mean velocity u_v of 26 m/s. Actually, this maximum in

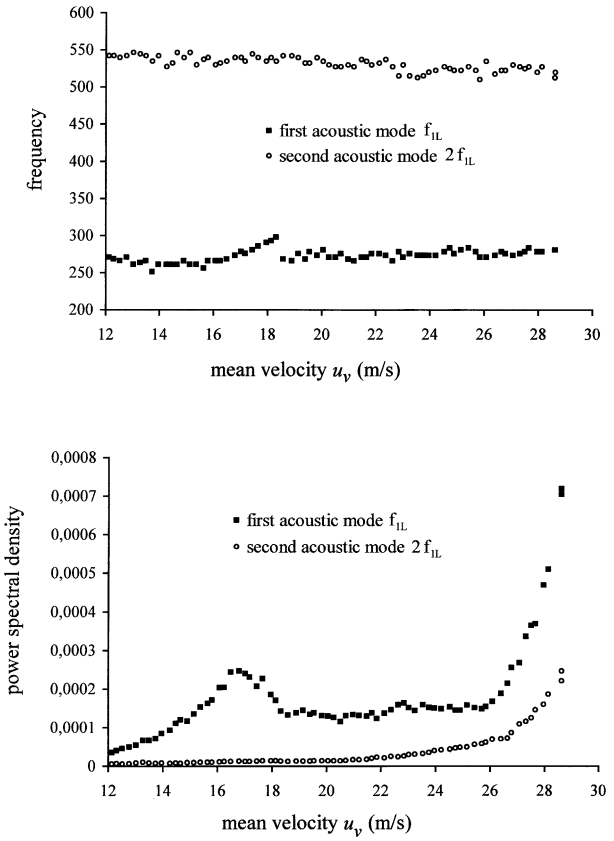

Fig. 4. Change of the magnitude and frequency of the most energetic frequency versus mean velocity level u_v.

magnitude appears with a frequency shift, close to the fundamental frequency. In fact, the frequency increases linearly by 40 Hz approximately and this linear evolution is obtained for $16 \leqslant u_v \leqslant 18$ m/s. Beyond $u_v = 18$ m/s, after an abrupt jump in frequency, no particular evolution of the fundamental frequency is observed.

To sum up, flow disturbances create pressure fluctuations in the whole chamber which correspond with the natural acoustic frequency. According to Plourde (1994), it is the presence of an obstacle that creates the development of a turbulent shear-layer in its wake. The non-linear nature of the evolution of the shear-layer may interfere with the pressure field. In fact, two different mechanisms are underlined with the pressure fluctuating study. A resonant phenomenon on the magnitude close to the fundamental frequency energy f_{1L} at Stage I as well as a large increase in fluctuating energy for the full range of frequencies at Stage II. The stability theory of Michalke (1972) states that the frequency of oscillations in the shear-layer depends on the impingement phenomenon. For a better understanding of the phenomenon, our experimental set-up intended to study the velocity fluctuations in the shear-layer as well as the possible links between the velocity and the pressure fluctuations.

3.2. Mean and fluctuating velocity field

The mean flow field has already been studied in previous works by Couton et al. (1996) and Plourde et al. (1996). These works mainly focused on the organisation of the whole flow in the chamber on both sides of the obstacle location with various injection wall conditions. All the experiments reported here were conducted with a porous plate of 2 μm sintered-bronze characteristic sphere diameter. This enables the whole chamber to be isolated from injection noise upstream of the injecting porous walls and avoids the dissipation of energy fluctuations in the chamber itself. Previous works showed that upstream of the obstacle location ($X < 0$), the flow was laminar with velocity distribution like Taylor's (1956) well-known analytical profiles, which were obtained for a simple geometry presenting no discontinuities.

In the wake of the obstacle, a turbulent shear-layer developed. Analysis of the fluctuating velocity spectra was important in order to understand the vortex shedding phenomenon and its potential link with the acoustic field. First of all, one might expect that the anemometer would respond to the acoustic velocity associated with the pressure wave. Quantitative analysis of the data reveals that this is not the case. As formerly indicated, the normalised pressure fluctuation amplitude at the head-end is 10^{-4} of the mean pressure. In such a condition, the amplitude of the acoustic velocity at the obstacle position would be approximately equivalent to $(a/\gamma)(\sqrt{P'^2}/P)$.

Fig. 5 shows the spectra of the anemometer wire downstream of the obstacle location outside and inside the shear-layer for $u_v = 27$ m/s. These data show that outside the shear-layer, the main energy organises itself at the first acoustic mode, at nearly 270 Hz while inside the shear-layer, the most energetic frequency is close to 480 Hz. Furthermore, energy contained at a frequency close to 270 Hz is much higher than that outside the shear-layer. For the spectrum obtained outside the shear-layer, the anemometer wire was located just above the shear-layer development, energy of the fluctuating

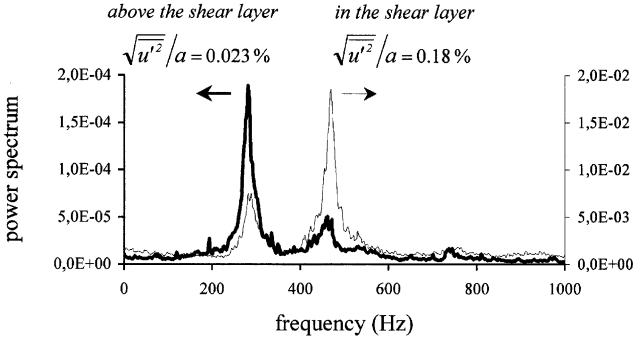

Fig. 5. Characteristic fluctuation velocity spectra in the obstacle area.

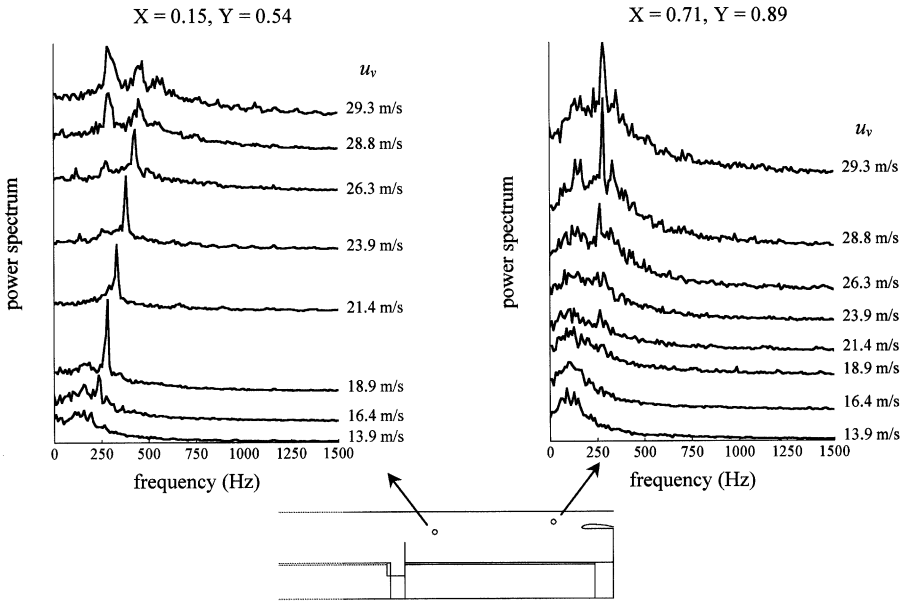

Fig. 6. Spectral analysis of fluctuation velocity component downstream of the obstacle position and its change with the mean velocity u_v.

velocity is 2.3×10^{-4} of the sound velocity while energy of velocity fluctuation is 1.8×10^{-3} of the sound velocity in the shear-layer ($X = 0.01$, $Y = 0.80$), that is nearly one order of magnitude higher. This suggests that the velocity fluctuations measured in the shear-layer correspond to a vortex creation. Fig. 6 presents the change of fluctuation velocity spectra as a function of u_v levels at two different locations in the shear-layer. The first location is at $X = 0.15$ and $Y = 0.54$, that is in the vicinity of the obstacle in the separated shear-layer region. A major change in spectra of responses is clearly identified. Although no particular peak is observed at low mean velocities such as $u_v = 13.9$ m/s, spectra are mainly characterised by a peak in magnitude at a frequency close to 250 Hz for $u_v = 16.4$ m/s. However, the frequency of this peak increases with rising u_v. For example, the dominant frequency is close to 270 Hz at $u_v = 18.9$ m/s and close to 450 Hz at 26.3 m/s. Concurrently, the magnitude of this peak is also a function of u_v. For $13.9 \leqslant u_v \leqslant 18.9$ m/s, magnitudes sharply rise and beyond $u_v = 18.9$ m/s, a slight decrease in the magnitude of the most energetic frequency is observed. For a mean velocity of 26.3 m/s, a second peak is present in the spectra at a frequency close to 270 Hz, which corresponds to the first longitudinal acoustic frequency. For mean velocity levels above 26.3 m/s, the most energetic peak occurs at a frequency close to the first longitudinal acoustic mode f_{1L} while the not-so-powerful second one is still present at 480 Hz. At $X = 0.71$, at which turbulence levels are higher, the spectra do not clearly present a dominant peak for velocity levels below 23.9 m/s. Although a peak does emerge at a frequency varying from 250 to 500 Hz, depending especially on the velocity level, spectra are mainly characterised by turbulent energy dissipation for a wide frequency range. When increasing mean velocity levels u_v, the energy of fluctuating velocities mainly organises itself at a frequency close to f_{1L}. It should be noted for the highest velocity that the dominant peak is sharper and centred at 270 Hz as if the coherence of the structures strengthens towards the downstream end of the channel.

Spectral analysis once again confirmed two different behaviour patterns of the entire flow depending on the level of u_v. Spectral responses were drawn over a wide range of mean velocity levels u_v at two different locations (see Fig. 7). More than 60 spectra for different velocity levels were used to draw it. This figure shows the change in the fluctuation velocity as a function of the frequency and the mean velocity level u_v. Magnitudes of the spectra are represented in grey; the darker the shades, the higher the magnitude. This pseudo-three-dimensional representation allows the most energetic frequencies and their evolution according to u_v to be extracted. Fig. 7a shows this pseudo-three-dimensional representation with velocity fluctuations recorded from a location close to the obstacle position while Fig. 7b presents measurements made at the rear end, close to the submerged nozzle.

In the vicinity of the obstacle, i.e. in the separated region, it is clearly evident that the most energetic frequency increased linearly while u_v increased from 12 to 30 m/s. The shear-layer organises itself at its natural frequency, depending exclusively on the hydrodynamic conditions. The higher the velocity, the higher the vortex shedding frequency. This behaviour has been well described in free mixing layers for example. As the natural destabilisation of the shear-layer reaches the natural resonant frequency of the whole chamber, around

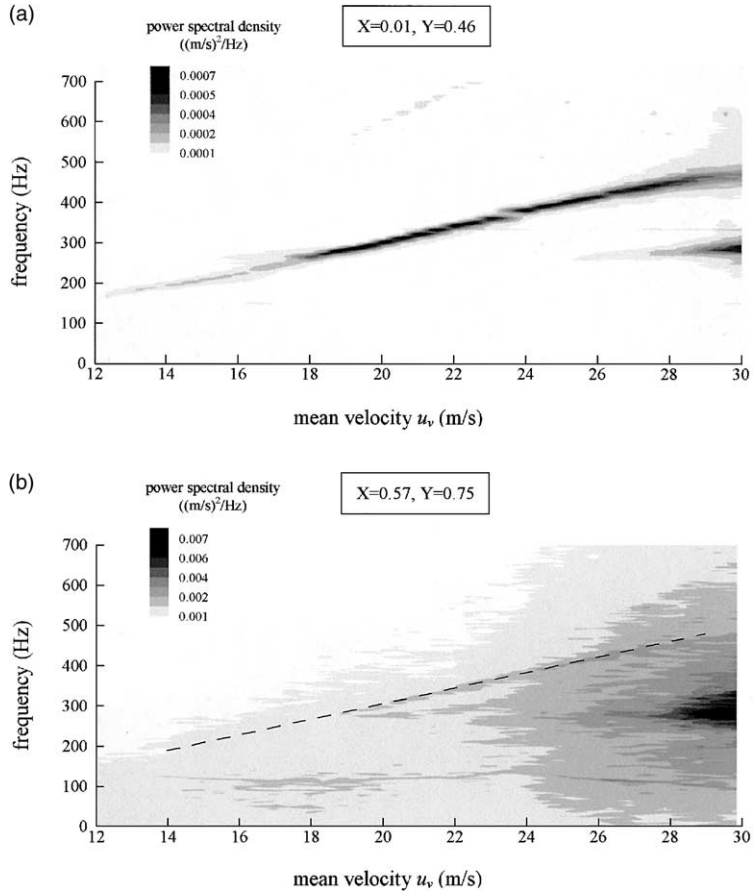

Fig. 7. Velocity spectral analysis with the mean velocity u_v at two different locations: (a) at ($X = 0.01$, $Y = 0.46$) near the obstacle location; (b) at ($X = 0.57$, $Y = 0.75$) in the rear-end.

270 Hz, a resonant phenomenon appears between the hydrodynamics and the acoustics. When u_v increases, the frequency of the vortex shedding also increases and then the resonant state forces the acoustic resonance to shift. The outcome is observed in Fig. 4 with a 40 Hz shift in the first acoustic mode. Over the same velocity range ($12 < u_v < 28$ m/s), the fluctuating velocity spectra do not present a particular energetic frequency at the rear-end of the chamber in Fig. 7b. This demonstrates that structures created in the separation zone lose their coherence on their way from the obstacle position to the submerged nozzle location. Structures created at a specific frequency in the separation zone are dissipated either by turbulence mixing or by interference with wall mass transfer; or the vortices are not initially sufficiently powerful to retain their coherence. The fact remains that the close link between acoustics and hydrodynamics diminishes rapidly. This is observed for the first acoustic mode jump obtained at $u_v = 18$ m/s. Beyond this velocity level, the vortex shedding frequency continues to increase up to $u_v = 28$ m/s. It is important to underline that at the rear-end, in this velocity range, although spectra are mainly characterised by turbulence dissipation, a low energy level is present at the same frequency as that of the vortex shedding frequency in the separation zone. This indicates that, under these conditions, structures are still present in the shear-layer and that a specific frequency emerges in the spectral response of the velocity fluctuations. A dotted-line is drawn in Fig. 7b in order to show this evolution. For $28 < u_v < 30$ m/s, the vortex shedding frequency suddenly jumps from 480 to 270 Hz as shown in Fig. 7a. In Stage II, the frequency of the most energetic peak does not vary. At the same time, as already observed in Fig. 6, energy fluctuations strengthen at a frequency close to the first longitudinal acoustic mode (270 Hz). This indicates that vortices in the shear-layer match up with the natural acoustics of the whole chamber and that a resonant phenomenon between the hydrodynamics and the acoustics interacts with the shear-layer. It seems that vortices are sufficiently powerful and manage to keep their coherence in spite of turbulence dissipation during their convection along the second injection block. The impingement of vortices upon the submerged nozzle creates noise at such a level that resulting pressure waves, travelling upstream of the flow, might have driven the vortex shedding phenomenon in the separation zone. Thus, to underline the close link between fluctuating pressure and velocity

fields, specific studies were conducted and are presented in the following section.

4. Identification of a coupling phenomenon

The study of velocity fluctuations, presented above, underlines the influence of the mean flow velocity in the chamber. The vortex shedding frequency is controlled by the flow dynamics as well as by vortex energy. In Stage II, where $26 < u_v < 30$ m/s, vortices are sufficiently energetic to keep their coherence between the obstacle location and the submerged nozzle position. The coherence of the structure is observed despite higher turbulence levels than those obtained in Stage I ($12 < u_v < 26$ m/s). As a result, the impingement of structures on the nozzle may provide a sufficient sound source to control the vortex shedding itself.

It is of interest to establish the link between the self-sustained shear-layer and the acoustics of the chamber. In order to quantify the link between the hydrodynamic and the acoustic fields, the temporal correlation coefficient of the pressure and the velocity fluctuations is defined as:

$$R_{u'P'}(\tau) = \frac{\overline{u'(t)P'(t+\tau)}}{\sqrt{\overline{u'(t)}^2}\sqrt{\overline{P'(t)}^2}} \quad (1)$$

This temporal correlation coefficient is also a spatial coefficient because the pressure fluctuations were recorded with the transducer located at the front-head of the chamber when the velocity fluctuations were measured in the shear-layer. For the evaluation of a possible feed-back loop, the pressure fluctuations at the front-head were compared with the velocity fluctuations, i.e. the hot wire was located at ($X = 0.71$, $Y = 0.89$) in the vicinity of the nozzle location. The characteristic change in $R_{u'P'}(\tau)$ levels for different mean velocities are shown in Fig. 8.

At $u_v = 15$ m/s, no strong correlation between the pressure fluctuations and the velocity fluctuations appears; $R_{u'P'}(\tau)$ does not exceed a 4% correlation and its evolution is mainly characterised by a regular trigonometric shape at a frequency close to the fundamental acoustic frequency (≈270 Hz). This particular shape is induced by the acoustic field, organised as shown before around the first acoustic longitudinal mode. For $u_v = 30$ m/s, correlation levels are higher and the shape of $R_{u'P'}(\tau)$ with a time delay τ shows two potential correlation times. The first one is located at approximately $\tau = -10$ ms and the second is identified at $\tau = 5$ ms. In fact, with increasing velocity u_v, two correlation areas are well observed with a negative time delay and a positive time delay. The values of the correlation coefficient are higher for the negative time delay τ^- than for the positive time delay τ^+. Pressure and velocity-fluctuation fields strengthen their correlation, reaching ≈14% at the negative time delay τ^- and more than 8% at the positive time delay τ^+. As observed in Fig. 8, it is difficult to establish the time delay τ for the highest correlation levels because of the trigonometric shape of $R_{u'P'}(\tau)$. Using the Hilbert's transform, the magnitude function $A(\tau)$ of the velocity–pressure correlation was calculated. In fact, a convolution integral of $R_{u'P'}(\tau)$ provided the Hilbert transform $\widetilde{R}_{u'P'}(\tau)$:

$$\widetilde{R}_{u'P'}(\tau) = R_{u'P'}(\tau) \times 1/(\pi\tau) \quad (2)$$

The magnitude function $A(\tau)$, also called the envelope signal of $R_{u'P'}(\tau)$, was calculated as

$$A(\tau) = \left(\widetilde{R}^2_{u'P'}(\tau) + R^2_{u'P'}(\tau)\right)^{1/2} \quad (3)$$

The envelope signal is drawn in dotted lines in Fig. 8. As the time delays vary widely with increasing u_v, the change of the correlation coefficient $R_{u'P'}(\tau)$ is drawn in Fig. 9 for a large range of u_v. In this pseudo-three-dimensional figure, the horizontal axis shows u_v and the vertical axis represents the time delay τ while the $R_{u'P'}(\tau)$ values are represented in different grey levels. Two

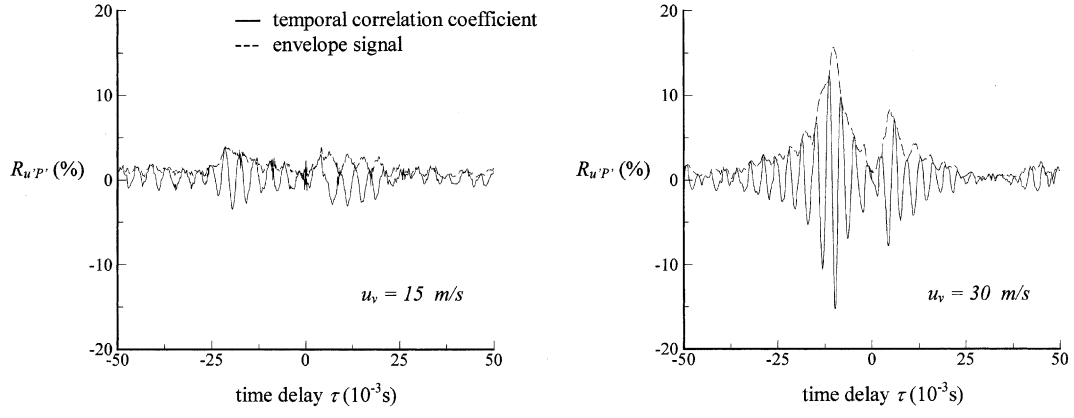

Fig. 8. Fluctuating velocity-pressure correlation coefficient at two different mean velocity levels u_v.

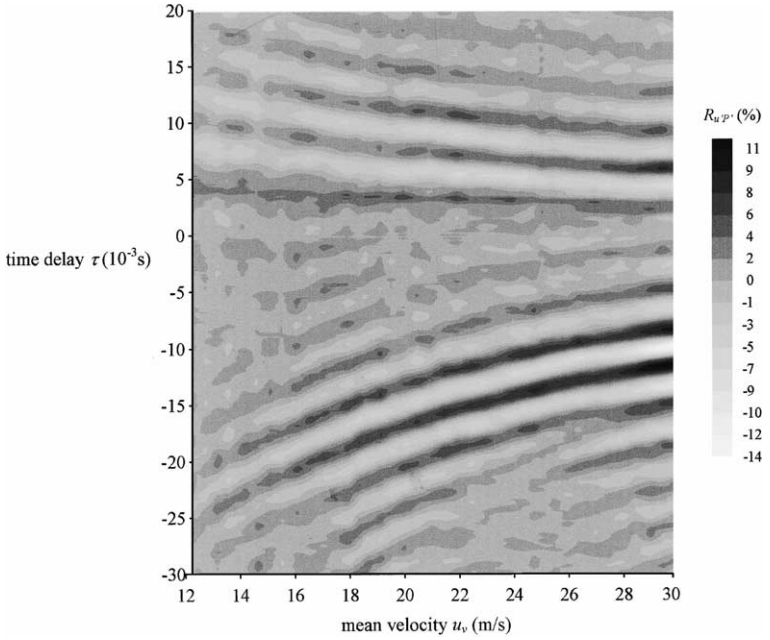

Fig. 9. Change of $R_{u'P'}(\tau)$ versus the mean velocity level u_v.

trends are clearly observed in Fig. 9. Firstly, the level of the mean velocity u_v is a determining factor in the correlation phenomenon between hydrodynamics and the pressure field. Moreover, a strong correlation at τ^- is observed with lower mean velocity levels u_v. For example, as soon as u_v reached 24 m/s, strong correlation coefficient levels are obtained, in contrast with that found with positive time delays. Secondly, it seems clear in Fig. 9 that the time delay, both for positive and negative values, varies with u_v. In fact, the higher the mean velocity the less the time delay. What is more, $R_{u'P'}(\tau)$ is significantly higher for positive time delays τ^+, over mean velocity limits of 28–30 m/s, the maximum velocity levels in such an experimental configuration. How can these two kinds of correlation be explained? In order to understand these mechanisms, an analytical model is tested to interpret the correlation data with some assumptions for τ^- and τ^+ time delays.

4.1. Model of correlation time delay

First, it is important to assume that the feed-back loop, as described by Ho and Nosseir (1981), is interfered with by the presence of a self-sustained shear-layer oscillation, within the mean velocity u_v range studied. Secondly, according to its definition, a strong correlation between the velocity fluctuations measured at the rear-end of the chamber and the pressure fluctuations from the front-head transducer at negative time delay τ^- indicates the correlated phenomenon occurs first at the front-head before the hot wire at ($X = 0.71$, $Y = 0.89$) detected it. Indeed, if a pressure wave creates a forced oscillation in the shear-layer resulting in the formation of a coherent eddy, this pressure wave would continue its convection at a velocity close to the sonic velocity a. Since pressure wave velocity exceeds by far the characteristic velocity of the structure, pressure fluctuations occur prior to velocity fluctuations. This is schematically indicated in Fig. 10 in which these features described above may be modelled as follows. Considering the velocity of the coherent structures u_c constant, the negative time delay τ^- can be written as

$$\tau^- = \frac{d_0}{u_c} - \frac{d_1}{a - u_v} \tag{4}$$

in which d_0 and d_1 are respectively the distance between the obstacle position and the hot-wire location and the distance between the obstacle and the front-head of the chamber. Although the mass flow rate is uniformly injected all along the chamber, i.e. the characteristic velocity increases linearly from the front-head to the rear-end, we assume as a first approximation that the ratio u_c/u_v is constant. Likewise, the positive time delay τ^+ can be modelled, assuming that the impinging structures upon the nozzle generate a sufficient noise to provide a driving pressure wave. In contrast to the negative time delay τ^-, the correlation at positive time delay τ^+ indicates the hot wire detects the correlated phenomenon ahead of the pressure transducer. Assuming that coherent structures are convected in the shear-layer, then impinge on the nozzle throat creating significant pressure waves, these waves travel upstream of the main flow before impinging on the front head (Fig. 10). So τ^+ may be modelled as

$$\tau^+ = \frac{d_2}{u_c} + \frac{d_3}{a - u_v} \tag{5}$$

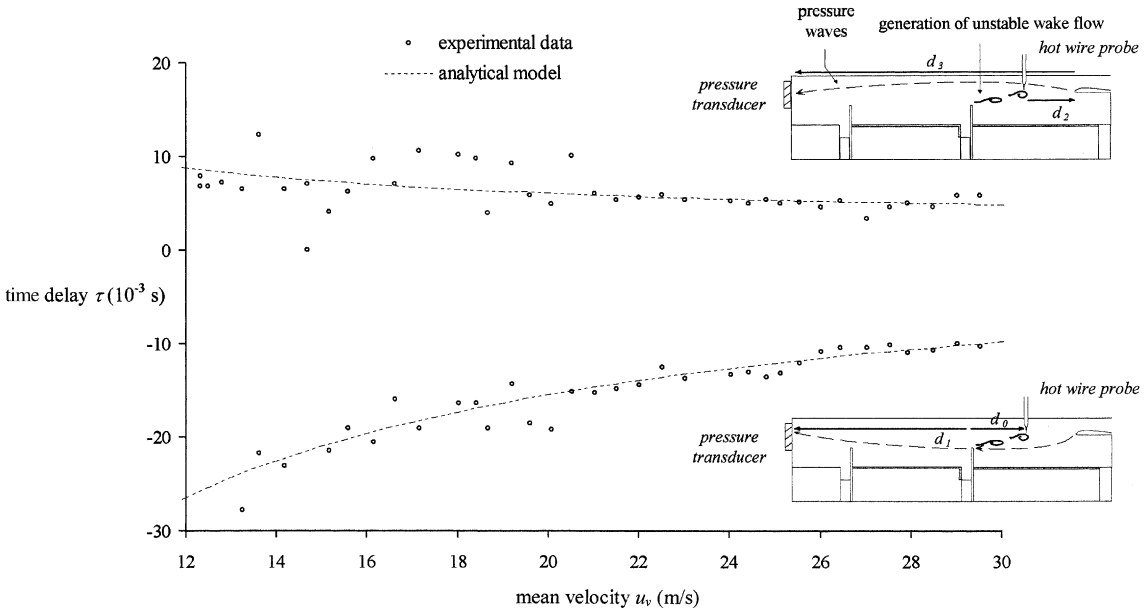

Fig. 10. Comparison between the experimental results of time delays and the analytical results.

in which d_2 represents the distance between the hot-wire location and the nozzle location and d_3 represents the distance between the front-end and the nozzle location. In order to check all the above assumptions, we compare both analytical τ^- and τ^+ models and the times at which a strong correlation is obtained.

Fig. 10 presents a comparison of experimental and analytical results of time-delay correlations. We first assume the presence of the feedback loop at every mean velocity level studied ($12 < u_v < 30$ m/s), so that expressions for τ^- and τ^+ have a physical meaning. Moreover, the convection velocity of structures is assumed to be constant and equal to 60% of the mean velocity level u_v. In fact, Ho and Nosseir (1981) found the convection speed of the large coherent structures to be 0.6 of the jet exit speed. Lau et al. (1972) or Neuwerth (1973) confirmed this value in a low speed and a high speed jet respectively. With these assumptions, equations for τ^- and τ^+ time delays were computed at the same location as the experimental velocity measurements. Results are shown by a dotted-line in Fig. 10. As already stated, the higher the velocity the smaller the time delay τ^+, as well as τ^-. The time delay at which the highest $A(\tau)$ envelope signal correlation is reached, is also shown in Fig. 10 by dots for both negative and positive time delays. It indicates good agreement between the experimental and analytical results; but as observed in Fig. 10, this agreement is achieved for both τ^+ and τ^-, beyond $u_v = 20$ m/s. As shown by the experimental results, τ^+ and τ^- correlation magnitudes become significant for $u_v = 24$ m/s and the feedback loop is present in the flow only at the highest velocity studied. This explains, then, why the analytical results were not in as good agreement in the low velocity range. Beyond $u_v = 24$ m/s, structures in the shear-layer are sufficiently powerful to keep their coherence. However, for $24 < u_v < 28$ m/s, impingement upon the sonic nozzle is not sufficient to force the vortex shedding frequency to match up with the acoustic waves, i.e. it is not strong enough to provide a feed-back loop. With higher mean velocities ($28 < u_v < 30$ m/s), more significant correlations are detected at τ^+, showing that impingement of coherent structures in these conditions generates energetic pressure waves, strong enough to force the vortex shedding at one of the acoustic modes. Correlation at τ^- are also consolidated as well as the pressure fluctuation field in the whole chamber. Thanks to the agreement with the simple analytical analysis, it is then clear that the feed-back loop generates a resonant state between the natural acoustic, coherent structures and self-sustained oscillations in the whole chamber. This is in fact responsible for the amazing agreement between the increase in the root-mean-square pressure measured at the front-head location and the corresponding vortex shedding frequency and the first longitudinal acoustic mode of the chamber.

5. Conclusion

Flow in a confined chamber with injection through porous walls was conducted in order to analyse the potential instability behaviour of the whole flow. Experiments were carried out at a constant mass flow rate fixing the Reynolds number of the flow. The characteristic internal velocity was varied over a range of 12–30 m/s, that is in very low subsonic range. First, it should be underlined that internal velocity is a predominant

parameter in the flow stability and two different trends are identified. Over the first velocity range (Stage I), coherent structures are produced in the separated shear-layer at a frequency that is independent of the natural acoustics of the chamber. Indeed, we show that the higher the internal velocity, the higher the vortex shedding frequency. The frequency varies over a wide frequency range, from ≈200 to 480 Hz. In fact, when the natural oscillation of the shear-layer is in the vicinity of the first longitudinal acoustic mode, it forces the acoustic frequency to increase with regard to the increase of the vortex shedding frequency. However, this link between the hydrodynamics and acoustics is not sufficiently strong to force a complete coupling of the flow. In fact, flow conditions cannot maintain the coherence of the structures. Turbulence in the shear-layer creates a high dissipation rate and vortices are dissipated in the wake of the obstacle. Then, no energetic coherent structures impinge upon the sonic throat, which could be a major source of noise. When mean velocity levels increase beyond 28 m/s, the structures are strong enough to keep their coherence from the obstacle to the rear-end of the chamber, i.e. from separation to impingement. Despite high turbulence rates in the wake of the obstacle, impingement of coherent structures at the rear-end of the chamber could strengthen the acoustics and then force the vortex shedding phenomenon to align with the pressure field. A coupling phenomenon between acoustics and hydrodynamics occurs generating a highly unstable development in this type of flow.

One of the major questions concerns the influence of the Reynolds number on this flow organisation as well as the influence of the injecting walls on the vortices. A non-linear amplification phenomenon may be observed with the increase of the internal mean velocity level in the chamber at a fixed mass flow rate, and thus for a particular Reynolds number, Re_c. As stated above, the Reynolds number is one of the most important parameters in the stability analysis of porous injecting walls and its influence could be important in the coupling phenomenon too. Moreover, in all the experiments presented herein, experimental conditions have especially forced the first longitudinal acoustic mode. However, it will be necessary to further analyse the effect of the predominant higher acoustic frequency on vortex shedding. Furthermore, turbulence could have an impact on the whole flow organisation. First, the impact of the injecting walls on turbulence development has not yet been studied; it could interact with the vortex shedding mechanism, i.e. with vortex coherence. Secondly, turbulence in such a flow is complex and occurs with a wide range of characteristic scales, whether hydrodynamic or acoustic scales. Within the scope of a solid propellant rocket motor study, it may be necessary to examine whether turbulence effects could be large enough to avoid the damage of a hydrodynamic–acoustic coupling.

Acknowledgements

This research was sponsored by the *Centre National d'Etudes Spatiales* (CNES). We give special thanks to Robert BEC, director of the Solid Propulsion Department, for his tireless aid.

References

Brown, R.S., Dunlap, R., Young, S.W., Waugh, R.C., 1981. Vortex shedding as a source of acoustic energy in segmented solid rockets. J. Spacecraft Rocket 18 (4), 312–319.

Couton, D., Plourde, F., Doan-Kim, S., 1996. Cold gas simulation of a solid propellant rocket motor. AIAA J. 4, 2514–2522.

Couton, D., Doan-Kim, S., Vuillot, F., 1997. Numerical simulation of vortex-shedding phenomenon in a channel with flow induced through porous wall. Int. J. Heat Fluid Flow 18, 196–283.

Couton, D., Plourde, F., Doan-Kim, S., 1999. Analysis of energy transfer of a sheared flow generated by wall injection. Exp Fluids 8, 222–232.

Dunlap, R., Brown, R.S., 1981. Exploratory experiments on acoustic oscillations driven by periodic vortex shedding. AIAA J. 19, 408–409.

Ho, C.M., Nosseir, N.S., 1981. Dynamics of an impinging jet. Part 1. The feedback phenomenon. J. Fluid Mech. 105, 119–142.

Hourigan, K., Welsh, M.C., Thompson, M.C., Stokes, A.N., 1990. Aerodynamic sources of acoustic resonance in a duct with baffles. J. Fluids Struct. 4, 345–370.

Isaacson, L.K., Marshall, A.G., 1982. Acoustic oscillations in internal cavity flows: non-linear resonant interaction. AIAA J., Tech. Notes 20, 152–154.

Lau, J.C., Fisher, M.J., Fuchs, H.V., 1972. The intrinsic structure of turbulents jets. J. Sound Vib. 22, 379–406.

Michalke, A., 1972. Instabilität eines Kompressibelen Runden Freihstrahls unter Berücksichtigung des Einflusses der Strahlgrenzschichtdicke. Zeit. Flugwissenschaft 19, 319–328.

Neuwerth, G., 1973. Akustiche Ruckkopplungserscheinungen am Unter-und Uberschall-Freistrahl, der auf einen Storkorper Trifft. Dr. Ing. Thesis. Tech. Hoschs Aachen, West Germany.

Plourde, F., 1994. Structures Turbulentes d'un Ecoulement Segmenté à Injection Pariétale. Ph.D. Thesis, University of Poitiers, France.

Plourde, F., Poisson, R., Doan-Kim, S., 1996. Space correlation measurements in a forced shear layer with wall injection. Exp. Fluids 21, 26–32.

Rockwell, D., Naudascher, E., 1979. Self sustained oscillations of impinging free shear layer. Ann. Rev. Fluid Mech. 11, 67–94.

Tang, Y.P., Rockwell, D., 1982. Instantaneous pressure fields at a corner associated with vortex impingement. J. Fluid Mech. 124, 307–334.

Taylor, S.G., 1956. Fluid flow in regions bounded by porous surface. Proc. Roy. Soc. Lond. A 232 (1199), 456–475.

Ziada, S., Rockwell, D., 1982. Oscillations upon an edge of an unstable mixing-layer impinging. J. Fluid Mech. 124, 307–334.